Analyst

PAPER

View Article Online
View Journal

Cite this: DOI: 10.1039/c6an00375c

Quantitative real-time detection of carcinoembryonic antigen (CEA) from pancreatic cyst fluid using 3-D surface molecular imprinting†

Yingjie Yu,*[a] Qi Zhang,[b] Jonathan Buscaglia,[c] Chung-Chueh Chang,[d] Ying Liu,[d] Zhenhua Yang,[a] Yichen Guo,[a] Yantian Wang,[a] Kalle Levon[b] and Miriam Rafailovich*[a]

In this study, a sensitive, yet robust, biosensing system with real-time electrochemical readout was developed. The biosensor system was applied to the detection of carcinoembryonic antigen (CEA), which is a common marker for many cancers such as pancreatic, breast, and colon cancer. Real time detection of CEA during a medical procedure can be used to make critical decisions regarding further surgical intervention. CEA was templated on gold surface (RMS roughness ~3–4 nm) coated with a hydrophilic self-assembled monolayer (SAM) on the working electrode of an open circuit potentiometric network. The subsequent removal of template CEA makes the biosensor capable of CEA detection based on its specific structure and conformation. The molecular imprinting (MI) biosensor was further calibrated using the potentiometric responses in solutions with known CEA concentrations and a detection limit of 0.5 ng ml^{-1} was achieved. Potentiometric sensing was then applied to pancreatic cyst fluid samples obtained from 18 patients when the cyst fluid was also evaluated using ELISA in a certified pathology laboratory. Excellent agreement was obtained between the quantitation of CEA obtained by both the ELISA and MI biosensor detection for CEA. A 3-D MI model, using the natural rms roughness of PVD gold layers, is presented to explain the high degree of sensitivity and linearity observed in those experiments.

Received 22nd February 2016,
Accepted 27th April 2016

DOI: 10.1039/c6an00375c

www.rsc.org/analyst

Introduction

Pancreatic cystic neoplasms represent precursors to pancreatic cancer. Mucinous pancreatic cysts are most likely to undergo malignant transformation, rather than non-mucinous pancreatic cysts; and therefore early detection and management of these cysts is critical.[1] Carcinoembryonic antigen (CEA) is a glycoprotein, which can be easily found in mucosal cells that line the walls of pancreatic cysts. CEA production is greatest in mucinous pancreatic cystic lesions, and thus used to help differentiate high-risk pancreatic cysts from those with low malignant potential.[2] Currently, the most common detection method for CEA is the enzyme-linked immunosorbent assay (ELISA), which is widely used for clinical detection. This method is fairly complex and takes at least ten hours to complete a series of steps leading to the final optical measurements. Furthermore, the equipment required is fairly sophisticated and not available in most hospitals. Consequently it may take several days to weeks to obtain the results.

Electrochemical technique has been widely considered as a strong alternative to conventional ELISA method for biomarker detection due to its lower cost, excellent rapidity and sensitivity.[3–10] Here we demonstrate that a potentiometric method which monitors the open circuit potential (OCP) variation upon protein binding to the sensing surface, can provide rapid and selective sensing whose accuracy is similar to ELISA, but requires only one tenth of the sample volume and obtain results within 20 minutes or less. The technique, based on a modified 3-D self assembled monolayer (SAM) molecular imprinting method, is robust, simple to implement, portable, inexpensive, and can be made readily available in the operating room or in any hospital and clinic. The use of SAMs for surface molecular imprinting of biosensor was first reported by Zhou *et al.*[11] They used octadecyltrichlorosilane (OTS) to imprint simple amino acids on a ITO glass, where they demonstrated that potentiometric detection was sufficiently sensitive to not only discriminate between different amino acids, but also discriminate between amino acids of similar structures,

[a]*Department of Materials Science and Engineering, Stony Brook University, Stony Brook, NY 11794, USA. E-mail: yuyingjie312@gmail.com, miriam.rafailovich@stonybrook.edu; Tel: +1 631 880 9687, +1 516-458-9011*
[b]*Department of Chemical and Biomolecular Engineering, New York University Tandon School of Engineering, Brooklyn, NY 11201, USA*
[c]*Department of Medicine, Stony Brook University School of Medicine, Stony Brook, NY 11794, USA*
[d]*ThINC Facility, Advanced Energy Center, Stony Brook, NY 11794, USA*
†Electronic supplementary information (ESI) available. See DOI: 10.1039/c6an00375c

but with different chiralities. Despite the promising results, this method had several drawbacks that prevented its implementation for the detection of more complex biological molecules. First, OTS is hydrophobic and soluble only in non-polar solvents, which makes it difficult to imprint most biological molecules that are hydrophilic. Second, while OTS reacts with the ITO to form MI sensors, those substrates are extremely flat. This limited their use to small molecules, whose radii were smaller than the thickness of the SAM, or at most 1.2 nm.[6,12–14] We show that these obstacles can be overcome if: (a) The SAM is coated on gold evaporated on Si rather than being directly coated on bare Si surface which is atomically flat (RMS roughness ~0.6 nm). In contrast to Si, which may have a single crystal surface, evaporated gold films form microcrystals and have an RMS roughness of 3–4 nm, which is similar to the dimensions of most protein molecules. This allows the proteins to be enveloped by the templating SAM and enables three-dimensional imprinting.[15] The latter greatly increases the accuracy of detection and the size limit of the molecule being detected.[16] (b) A far larger range of SAMs with different functionalities is available when thiol rather than trichlorosilane chemistry is used. Thiol, end functionalized with OH group, is hydrophilic and can be dissolved together with a much large range of biological molecules, such as enzymes, viruses, bacteria, and proteins. Wang *et al.*[17] demonstrated the ability of this technique to detect and differentiate between poliovirus and adenoviruses, as well as between other proteins such as hemoglobin and myoglobin.[16] Yet, despite its promise, the method had not been applied "*in vivo*" to actual physiological fluids, where its sensitivity and selectivity could be probed in the presence of multiple other factors present in bodily fluids and where the results could also be verified using standard methods in an independent pathology laboratory. In this paper we probe the clinical relevance of the potentiometric method by using it to evaluate the CEA concentration in pancreatic cyst fluid obtained from 18 patients, under IRB 95867-6. Pancreatic cysts are frequently observed inadvertently during clinic procedures and having an immediate analysis of their CEA content. CEA was selected as our probe, due to its availability in highly purified form and its physiological importance as a marker for colon, breast, and pancreatic cancers. We used the potentiometric sensing to measure the amount of CEA present in wet biopsies taken from the pancreatic cysts and then compared the results with those obtained using ELISA from the hospital pathology laboratory. Excellent agreement between two methods proves the accuracy of MI biosensor.

2. Experimental section

2.1 Materials

11-Mercapto-1-undecanol ($SH–(CH_2)_{11}–OH$), dimethyl sulfoxide (DMSO), potassium ferricyanide ($K_3[Fe(CN)_6]$), potassium ferrocyanide ($K_4[Fe(CN)_6]$), matrix metalloproteinase-7 (MMP-7), CEA from human fluid, human CEA ELISA kit were all purchased from Sigma Aldrich. Gold/chromium (100 nm/10 nm) coated on silicon wafer substrate fabricated in the Cornell NanoScale Facility. Dulbecco's Phosphate-Buffered Saline (DPBS) buffer was used as detection solution for all the tests.

2.2 Fabrication of MI biosensor

Gold/chromium (100 nm/10 nm) coatings on single crystal [1,0,0] silicon wafers were prepared using electron beam evaporation at a vacuum of 10^{-7} Torr in the Cornell NanoScale Facility. The chromium layer was to improve the adhesion of the gold to silicon substrate. The gold-coated substrate (1.5 cm × 2 cm) was rinsed with ethanol and dried under nitrogen gas before use. In order to keep the working area of each gold substrate constant, the teflon tape with an 1.26 cm diameter hole made by a hole puncher is adhered to the gold surface. The mixture of thiol/DMSO and protein/DI water with proper ratio were prepared as imprinting solution to make well-ordered SAM on gold surface. Thiol and protein mixtures were made as follows: the template molecules (CEA) were dissolved in deionized water with a series of concentration. The alkanethiols, were dissolved in DMSO. The two solutions were then mixed at 19 : 1 (v : v) respectively to make 100 μM final thiol concentration. The prepared gold-coated chip was immersed into blend solution at room temperature for 2.5 hours and soak into 1 M NaCl aqueous solution for 1 hour to remove the template molecules.

2.3 Open circuit potential (OCP) detection system

CEA was assayed in a beaker containing 10 mL of 1× PBS detection medium. Open circuit potentiometer (Lawson Laboratories, Model E13) was utilized to measure the potential change of the biosensor without applying external electric field. An Ag/AgCl electrode (BASi) was connected to reference channel and the imprinted Au/Cr/Si chip was connected to working electrode channel. A fixed amount of the analyte solution was pipetted dropwise into the detection medium, and the open circuit potential (OCP) change was monitored and the analyte detection process was recorded using L-EMF DAQ software.

Cyclic voltammetry (CV) and electrochemical impedance spectroscopy (EIS) measurements were performed using a CHI 660d electrochemical workstation (CH Instruments) with a three electrodes system. It consists of a gold chip electrode, with or without molecular imprinting, as the working electrode, a platinum wire as the counter electrode and an Ag/AgCl electrode as the reference electrode.

3. Results and discussion

3.1 Model of the CEA MI process

The basic mechanism for MI mechanism is illustrated in Fig. 1. CEA, as the analyte in this study, can be viewed as a rod shaped molecule with 9 nm diameter.[18] CEA molecules are adsorbed simultaneously with the thiol molecules onto the

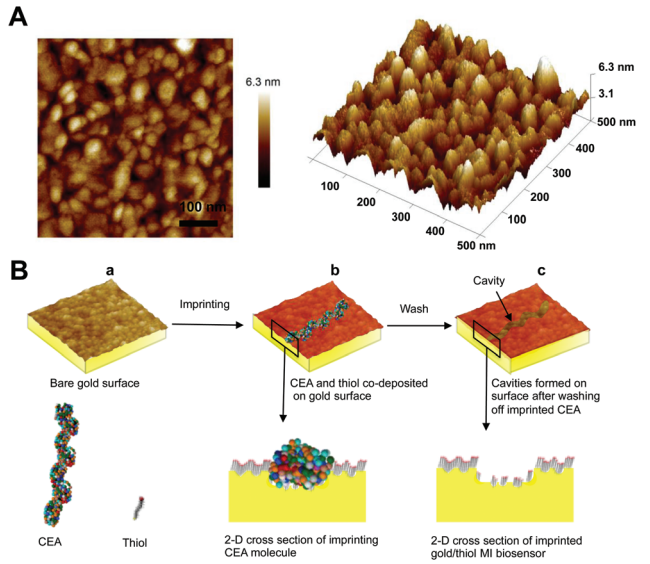

Fig. 1 (A) 2D and 3D AFM image of bare gold. (B) Schematic illustration and cross-sectional of the 3-D MI biosensor fabrication process. The red-color layer represents SAM coverage.

gold-coated Si chip to form a self-assembled monolayer. The new mechanism for surface MI, differs from the one previously proposed,[11] where it was assumed that the thiols were adsorbed together with the analyte on an atomically flat surface where a monolayer was formed around the analyte. In that model the templating was determined only by the size of the thiol molecules, which was a maximum of 2 nm.[16] This model worked well when the templating was performed on atomically flat surfaces, such as those of native oxide covered Si and the analytes were small molecules, such as methylphosphonic acid (MPA).[19] Hence it was very difficult to explain how imprinting with proteins larger than 10 nm, or nearly ten times larger than the thiol molecule, could discriminate between hemoglobin and myoglobin, as previously reported.[16,17] We propose an alternate quasi-3D molecular imprinting model as shown in Fig. 1(B). In contrast to native oxide coated Si, physical vapor deposition (PVD) of the gold substrate results in micro crystalline films with surface roughness of approximately RMS ~ 3–4 nm, as shown in the AFM scan in Fig. 1(A). The co-adsorption process of thiols and proteins on these surfaces is illustrated in step b in Fig. 1(B). The thiols adsorb to the gold surface and form a closely packed crystalline layer, which, as shown in side view of Fig. 1(B), is conformal to the morphology of the gold surface. During the co-adsorption process, CEA fits into one of the crevices formed on the gold surface. The thiol molecules, which are adsorbed at the same time, fill in the spaces "fitting" the CEA molecules accurately into the space provided through H-bonding from hydroxyl groups or hydrophobic interaction between the thiol chain and template protein. The imprinting molecules are then removed by soaking the chip in 1 M NaCl for one hour, leaving behind the specific three dimensional cavity imprint as shown in Fig. 1(B) step c. When the sensor is next exposed to the detection solution, only the molecules fitting precisely into the three-dimensional imprinting pattern can fit and trigger the potential response.[20]

Each step of molecular imprinting process on the gold surface was monitored through CV and EIS.[21,22] CV was employed here to investigate the effect of adsorbed thiol and protein layer on electron transfer between the gold electrode and electroactive moieties in solution, namely, $[Fe(CN)_6]^{4-}$and $[Fe(CN)_6]^{3-}$. In Fig. 2(A), before imprinting, conductive bare gold surface facilitate electron transport, and producing an apparent pair of reversible $Fe(CN)_6^{4-/3-}$ redox peaks at E_{pa} of 0.321 V and E_{pc} of 0.167 V. After imprinting, the anodic and cathodic peaks disappeared which resulted from a decrease in the electron transfer rate constant due to a condensed non-conductive thiol/CEA layer formed on the gold electrode surface. This layer act as a barrier, which prevents the redox active metal ions from approaching the electrode surface. To further remove the template CEA molecules, the imprinted electrode was soaked in 1 M NaCl for one hour, which is the optimal method selected to remove the CEA templating molecules (Part 1 in ESI†). The redox peaks re-appear, suggesting the successful removal of the CEA template and increasing of area exposed on the gold surface. Finally, upon the addition of 8.5 ng mL^{-1} CEA to the solution, the redox current was again reduced, with E_{pa} and E_{pc} shifted to 0.314 V and 0.125 V, which suggested an efficient recognition of CEA by a large faction of the cavities and a partial occupation of those by the CEA molecules.

In the EIS experiment (Fig. 2B), bare gold substrate displayed a straight line, corresponding to a mass diffusion-limited electron transfer process. After the co-deposition of thiols and CEA, the straight line was converted to a well-defined semicircle, characteristic of the largely increased electron transfer resistance, R_{et}. The subsequent removal of CEA templates by 1 M NaCl significantly reduced the semicircle, indicating the exposed gold surface in the molecular imprint-

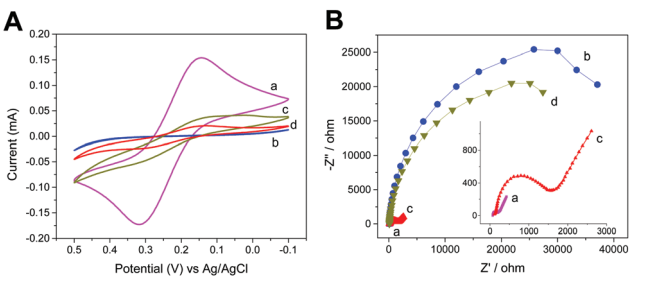

Fig. 2 (A) Cyclic voltammograms (CV) of the different electrodes (a) bare gold, (b) after CEA imprint, (c) after washing, (d) after addition of CEA (8 ng ml^{-1}): scan rate, 0.1 V s^{-1}. (B) Electrochemical impedance spectra (EIS) of different electrodes: (a) bare gold, (b) after CEA imprint, (c) after washing, (d) after addition of CEA (8 ng ml^{-1}). Inset: EIS of (a) bare gold (c) and after washing. EIS was tested with 5 mV amplitude and frequency range of 0.1–100 000 Hz. Both CV and EIS were performed in KCl solution (0.1 M) containing $[Fe(CN)_6]^{4-}/[Fe(CN)_6]^{3-}$ (5 mM).

ing cavities, when the re-addition of CEA would increase R_{et} again due to the reoccupation of the cavities by CEA. This trend nicely agrees with what we observed with CV and clarifies the working mechanism of CEA MI biosensor as illustrated in Fig. 1(B).

3.2 Estimation of CEA absorption on gold surface

In order to optimize the imprinting process we first determined the adsorption isotherm of CEA onto the gold surfaces. Solutions of CEA in concentrations of 5, 10, 15, 20 ng ml^{-1} were prepared in DI water, and in blend thiol/CEA imprinting solution respectively. Cleaned bare gold chips with same working area were immersed into either CEA/DI or CEA/thiol/DI blend solutions for 2 hours to let the CEA molecules absorb fully to gold surface. After the absorption process reached equilibrium, the amount of CEA remaining in solution, R, was measured using ELISA. The results are shown in the inset to Fig. 3A, where we plot the original amount of CEA mass in the solution, R, *vs.* the mass of CEA adsorbed on the gold surface, or $(1 - R)$. From the figure we can see that below 100 ng of CEA imprinting mass the two curves are nearly identical, where the adsorbed concentration increases linearly with the total CEA mass in solution. Above this concentration, the solution in DI increase with a slightly smaller step, while the solution containing thiol saturates, due to the thiol molecules competing for the surface area on gold with CEA molecules.

3.3 Optimizing the OCP response *vs.* CEA concentration curve

In order to achieve the largest OCP response signal for CEA addition, the surface molecular imprinting condition has to be optimized. In Fig. 3(B) we plot the OCP change of the CEA biosensor as a function of CEA addition in testing medium. CEA sensors were fabricated in 4 different CEA imprinting concentrations, 5, 10, 15, and 20 ng ml^{-1}. The typical OCP response of the CEA MI biosensor curve composed of a linear region where the OCP change is directly proportional to the analyte CEA concentration in testing medium. This region is followed by an abrupt transition to a plateau region, where the OCP response remains fairly constant despite increasing analyte concentration.

In the linear region, the imprinted cavities are being filled by the analyte CEA molecules, where the OCP change gradually increases due to the electron current generated by the number of cavities filled by CEA. The linearity of the OCP change is an indication that minimal overlap occurs in filling the imprinted cavities. Once all the cavities are filled, the OCP response is kept the constant with the increasing of CEA addition, as the gold surface saturation occurs at this CEA imprinting concentration.

The dynamic range of CEA biosensors also increased with the imprinting concentration of CEA. The widest dynamic range, from 0 to 8.5 ng ml^{-1}, can be obtained at CEA imprinting mass of 15 ng ml^{-1}. Once all the cavities are filled, the OCP response no longer increases since the gold surface is now fully covered by CEA and/or thiol molecules. The slope of

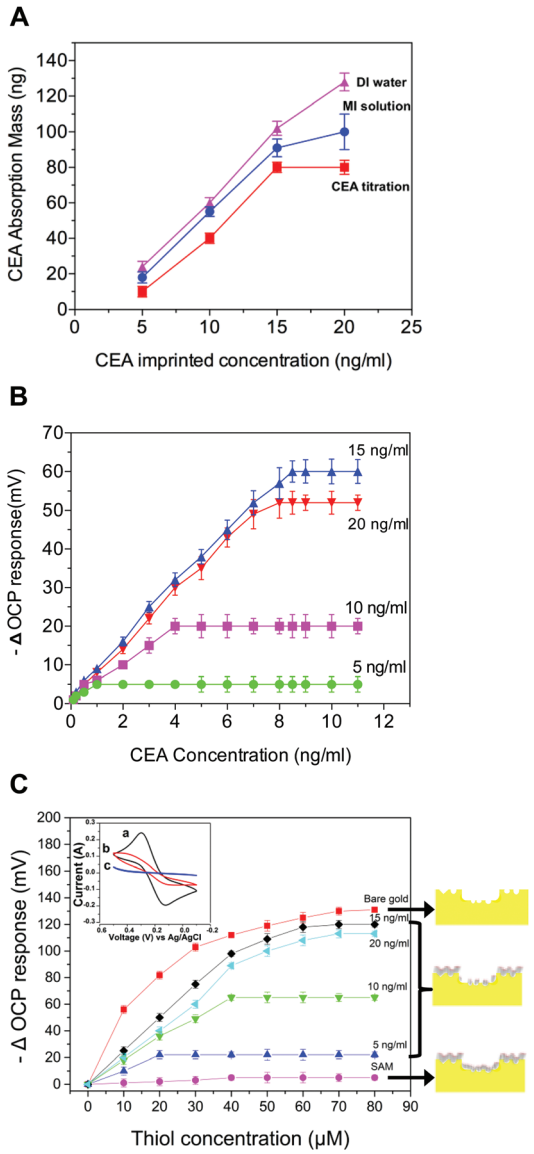

Fig. 3 (A) The amount of adsorbed CEA mass as a function of the CEA concentration in the MI solution and DI water, as measured *via* ELISA or inferred from the CEA titration experiments. (B) OCP response of the electrodes imprinted at four different CEA concentrations, as shown in the figure legend. Note all curves have a linear and a plateau region. (C) Thiol titration: OCP response as a function of thiol concentration added into testing solution on an imprinted gold electrode, as illustrated in the schematic adjacent to the figure. Inset: CV of bare gold and SAM. Imprinting and detection were performed in a 10 ml volume.

the OCP response and the CEA concentration curve in the linear region determines the sensitivity of the biosensor. The larger the slope of the linear region and the higher the maximum value, the more sensitive and wider the dynamic range of the biosensor. A clear maximum response occurs at 15 ng ml^{-1}. The slopes of the curves at 15 and 20 ng ml^{-1} are nearly the same, but the linear range at 15 ng ml^{-1} is wider, indicating that overlap of the imprinted areas begins to occur at higher concentrations. From the optimization curve, both

the maximum OCP response and the slope increase with CEA imprinting concentration until 15 ng ml^{-1}, suggesting the largest number of cavities created at 15 ng ml^{-1} CEA imprinting condition. Therefore, 15 ng ml^{-1} CEA concentration is the optimal imprinting condition to generate the largest OCP response for the CEA biosensor.

The formation of cavities by the imprinting method can be confirmed by titrating the gold surface after removal of the imprinted CEA molecules. It is well established that thiol molecules are adsorbed to the gold surface through strong sulfur–Au bond to form self assembled monolayers (SAMs) *via* the electron transfer reaction,[23,24] R–S–H + Au → R–S–Au + e^- + H^+. Therefore the adsorption process could be studied by observing the OCP generated during the thiolation process, which could provide a qualitative confirmation of the exposed gold area created by washing off the imprinted CEA. In order to determine the OCP generated to fully cover the bare gold electrode, a thiol/DMSO solution with concentration of 0.4 mg ml^{-1} was prepared and gradually added into the testing solution. The curves are shown in Fig. 3(C), a plateau value of 120 mV is obtained at a titration concentration of 70 μM for thiol titration on bare gold surface, corresponding to the maximum coverage of the exposed free gold area on the gold surface.

However, when we titrated same thiol solution to a well-incubated 100 μM thiol layer, no obvious OCP response is observed due to the insulating thiol layer block the electron transfer during thiolation process. The other curves shown in Fig. 3(B) correspond to titration of electrodes, which had been imprinted with different CEA concentrations, and then removed the template CEA. The OCP response on these curves is assumed to increase with thiol concentration till the exposed areas are fully covered, which means a dense insulating SAM layer formed on the gold surface. From the thiol titration process, the largest number of CEA imprinting cavities formed at the 15 ng ml^{-1} CEA imprinting condition, which confirms the CEA optimal imprinting as shown in Fig. 3(A). The side view of the process for each curve is compared schematically in Fig. 3(C) where arrows point to selected curves corresponding to the illustrations. At the two extremes, the bare gold surface corresponds to the blank gold surface without SAM formation, while the one exposed to the 100 μM thiol solution corresponds to the surface fully covered with an SAM. The curves in between correspond to the geometry where bare gold areas become exposed within the SAM after the imprinting CEA molecules are removed. This model is further confirmed using CV (shown in the inset), where a large redox peak is observed on the bare gold surface. Exposure of the electrode to 50 μM thiol solution produces partial coverage and reduces the redox peak, while exposure to 100 μM solution nearly eliminates the signal, consistent with formation of an insulating SAM.

We can estimate the number of CEA molecules that participated in forming the imprinted region on the electrode from the CEA mass at the saturation point of the response curve. This value represents the maximum amount of CEA molecules required to fit into the cavities of CEA biosensor. In the linear regime, each CEA molecule contributes the same amount of charge, and hence the potential increases linearly with concentration. Once all the exposed gold surfaces are filled, other molecules are adsorbed on the thiol layer, and generate far less charge. The concentration of CEA at the intersection of the linear and plateau regions corresponds to the mass of CEA or the number of molecules required to fill all the voids left by the imprinting process. The results are plotted in Fig. 3(A) as a function of the CEA imprinting concentration, indicating the mass of CEA which is available for detection is smaller than mass of the CEA adsorbed onto the gold during the imprinting process.

3.4 Re-usability, stability, and storage of MI biosensor

The good agreement between the ELISA and titration results also raises the question as to how many times can adsorbed CEA be removed form the imprinted regions, *i.e.* how many times can the imprinted sensor be washed and re-used before degradation in performance occurs?

In Fig. 4(A) we show the OCP response curves obtained from a chip imprinted at a optimal CEA imprinting concentration of 15 ng ml^{-1} after the first use, followed by soaking in 1 M NaCl for one hour to remove imprinted CEA, and exposing again to the detection solution to follow the same CEA measurement procedure as before. From the Fig. 4(A) we can see that small degradation occurs after the first two uses. Using the same chip a third time though shows obvious deterioration. The slope of the OCP response curve did not decrease a lot, but the saturation concentration decreased from 8.5 ng ml^{-1} to 4 ng ml^{-1}. This decrease is due to that after 3 detection–washing cycle of CEA molecule into the cavity of the sensor, the quality of the SAM decreased, resulting in the shrink of the dynamic range of the CEA sensor. In the inset of Fig. 4(A), the OCP response of the sensor gradually decreased with the increasing use cycles, and ultimately disappeared after the fourth attempt.

Stability can also be measured by determining the length of time that the chip can be used without degradation after the imprinting occurred. Chips were imprinted with CEA and tested with analyte immediately or after 24, 48, 72 and 96 hours. Three methods of storage were used during these periods, desiccator (100 Torr), ambient air, and submerged in DI water. According to the results, shown in Fig. 4(B), when stored in a desiccator, minimal degradation occurred up to 48 hours and only partial degradation was observed after 72 hours. Storage in DI water incurred a 50% decrease in potentiometric sensitivity within the first 24 hours, while storage in ambient conditions resulted in a loss of nearly 70% within the first 24 hours. CV of the surfaces obtained after 72 hours indicated that the surfaces were still fully covered with thiols. Hence no displacement of thiols occurred either in water or air, as expected given the strength of the gold–sulfur bond. The large difference between the samples stored in vacuum *vs.* those stored in air or water indicated that the

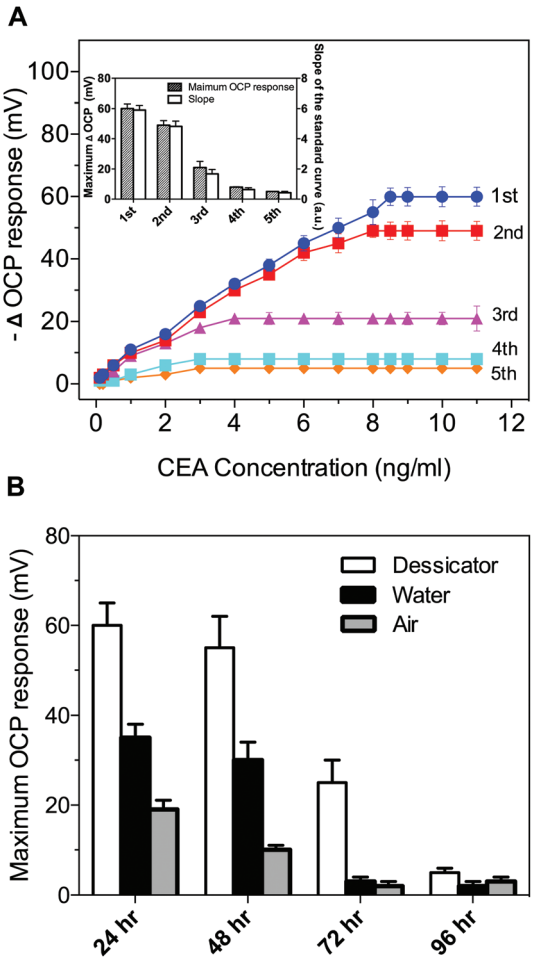

Fig. 4 Stability testing of the MI biosensor: (A) OCP response of a CEA molecular imprinted biosensor after multiple repetitions of the detection/wash cycle. Inset: Maximum OCP response and slope of OCP response curve *vs.* cycle number (B) The slope and maximum OCP response for CEA imprinted sensors after storage in a vacuum desiccator, DI water, and air for up to four days.

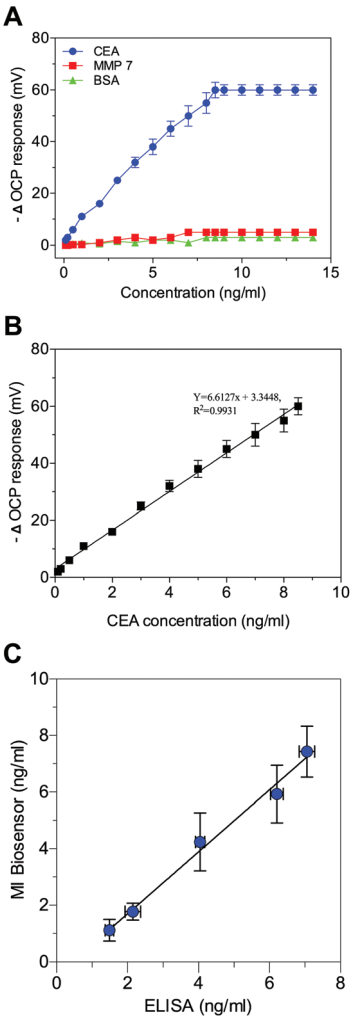

Fig. 5 (A) CEA MI biosensor selectivity test: OCP response of the sensor imprinted with CEA and tested with MMP 7, BSA, respectively. (B) OCP response of the MI biosensor after addition of CEA in the linear response region. (C) Calibration of the CEA imprinted sensor: MI reading of known concentration of CEA *vs.* ELISA reading of the concentration.

most probable mechanism for the decrease in performance was due to surface contamination of the hydroxyl groups.

3.5 Calibration and selectivity test of CEA MI biosensor

In order to obtain absolute readings of the CEA concentration and compare them to those obtained using ELISA analysis, a two-step calibration process was followed. First, the potentiometric response obtained from the MI biosensor was calibrated against aliquots of known concentration. The results shown are Fig. 5(A) where the response function is observed to have two distinct regions, a linear region and a plateau region. The OCP response corresponding to a given analyte concentration in the test solution can be obtained by fitting the linear region, as shown in Fig. 5(B).

Second, samples of known CEA concentration were analyzed using both ELISA and the biosensor. The values obtained from the biosensor output were plotted *vs.* those obtained with the ELISA reader in Fig. 5(C). Even though the data are well fit be a linear relation, the ELISA readings were consistently larger by 9%.

The selectivity of the biosensor imprinted for CEA was further confirmed by cross testing with matrix metalloproteinase-7 (MMP-7) and bovine serum albumin (BSA). MMP-7 is another commonly used tumor marker with similar size as CEA. Serum albumin is the most abundant blood plasma protein in mammals. Therefore, eliminating the noise of serum albumin is very important for application of biosensor to patient cyst fluid. In Fig. 5A, we find that no OCP response is observed in the absence of CEA.

3.6 Usage under physiological conditions

Patients presenting to Stony Brook hospital's endoscopy unit for pancreatic cyst evaluation by means of endoscopic ultrasound (EUS) were enrolled for study (IRB#95867-6). As standard of care at the time of this study, EUS-guided fine needle

aspiration (FNA) was performed of all pancreatic cysts greater than 1–2 cm in size, or those lesions with high-risk morphological features previously observed under ultrasound. The endoscopic technique of EUS-FNA has been previously described.[1] Fluid was aspirated from the cyst cavity using a through-the-scope 25 gauge or 22 gauge FNA needle. The fluid was then sent to the hospital pathology laboratory where it was analyzed for cytological content and morphology, as well as the level of amylase and CEA by the means of ELISA. An additional 0.5 ml of pancreatic cyst fluid was collected for study purposes which was immediately centrifuged in order to separate cyst fluid content from red blood cells, and stored in a freezer at −80°. The CEA content of the cyst fluid was determined by thawing the samples and adding 10 microliters of cyst fluid into a total volume of 10 ml of PBS. The solution was further diluted till the OCP reading was in the linear range of the sensor. A set of MI biosensors was fabricated according the protocols described previously. Two readings from two different imprinted sensors were taken from each patient. The CEA concentration was determined from the OCP response using the calibration curve established above and correcting for the ELISA offset. The average values and corresponding standard deviations are plotted in Fig. 6. The concentration of cyst fluid samples ranged over three orders of magnitude, where the highest readings were obtained from patients diagnosed with adenocarcinoma. The data obtained from MI biosensor can be fitted with ELISA data in a straight line, having a slope 1.011 (95% confidence interval M = 0.9943 to 1.028, Chi^2 = 0.9157). In order to ensure that the fitting parameters were indeed consistent over the entire range, the low concentration region, outlined in the red box of the figure was fit separately as well and is plotted in the inset of Fig. 6. The slope obtained, 1.016 is not significantly different than that obtained over the whole range, 1.011. These results indicate that the response of the sensor is highly linear over a very large concentration range and the calibration procedure relative to the ELISA method outlined above is accurate and reproducible (n > 40 trials). Furthermore, the accuracy of the results is comparable to that obtained with ELISA, yet the volume of fluid used ranged from a maximum of one hundred microliter at the lowest concentrations to 10 microliters in the cancerous cysts, as compared to a volume of at least 150 microliters required for the ELISA test. In addition, the results were obtained in 5 minutes, as opposed to a minimum of 10 hours, required by the ELISA test. Hence the accuracy and the analysis time for this sensor are ideal for use at bedside and can allow the physician to make an informed decision regarding the potential malignancy of the cyst. In case the cyst is malignant or simply to minimize the disturbance of the cyst the smaller volume required for analysis is a distinct advantage.

Finally, these results also indicate that the biosensor was able to maintain its selectivity for CEA despite the presence of many other proteins and markers in the cyst fluid.[25] Despite the accuracy of the sensor in detecting a single analyte, confidence in the determination of malignancy requires simultaneous detection of multiple analytes. These results confirm that this can be accomplished by combining several sensors, imprinted for different markers, whose response can be multiplexed and recorded separately as part of a chip based sensing array. The authors declare that all patient samples were taken with permission in accordance with the ethical guidelines of Stony Brook University using a protocol approved by the Institutional Reveiw Board (IRB 95867-6, October 27, 2010).

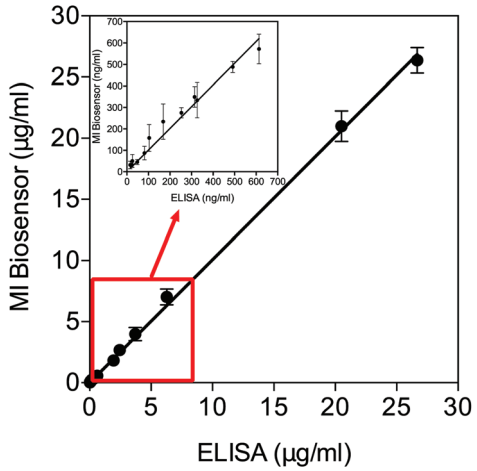

Fig. 6 CEA concentrations in the pancreatic cyst fluid from 18 patients. The MI biosensor reading plotted *vs.* the ELISA reading of the samples obtained from the official pathology report. Inset: Magnified section of the points near the origin.

4. Conclusion

In conclusion we have shown that a MI biosensor can be constructed whose accuracy for the detection of CEA in pancreatic cyst fluid obtained from 18 patients is comparable to that obtained by ELISA over a concentration range spanning nearly three orders of magnitude. We also showed that this biosensor could be used at bedside since the measurement required only 1% of the volume needed for the ELISA determination and the results were obtained within 5 minutes using a portable potentiometer. Hence this sensor can allow the physician to make a rapid diagnosis as to further treatment of cysts which were discovered incidentally during other procedures.

Acknowledgements

We greatfully acknowledge the support of the National Science Foundation (NSF grant INSPIRE#1344267).

References

1 W. R. Brugge, K. Lewandrowski, E. Lee-Lewandrowski, B. A. Centeno, T. Szydlo, S. Regan, C. F. del Castillo, A. L. Warshaw and I. C. Study, *Gastroenterology*, 2004, **126**, 1330–1336.

2 Z. H. He, N. Gao and W. R. Jin, *Anal. Chim. Acta*, 2003, **497**, 75–81.
3 D. R. Thevenot, K. Toth, R. A. Durst and G. S. Wilson, *Biosens. Bioelectron.*, 2001, **16**, 121–131.
4 W. C. Mak, K. Y. Cheung, D. Trau, A. Warsinke, F. Scheller and R. Renneberg, *Anal. Chem.*, 2005, **77**, 2835–2841.
5 F. Ricci, G. Adornetto and G. Palleschi, *Electrochim. Acta*, 2012, **84**, 74–83.
6 Q. Zhang, A. Prabhu, A. San, J. F. Al-Sharab and K. Levon, *Biosens. Bioelectron.*, 2015, **72**, 100–106.
7 M. S. Wilson and W. Y. Nie, *Anal. Chem.*, 2006, **78**, 2507–2513.
8 J. Wang, *Biosens. Bioelectron.*, 2006, **21**, 1887–1892.
9 J. H. Chen, Y. L. Zhou, D. H. Wang, F. He, V. M. Rotello, K. R. Carter, J. J. Watkins and S. R. Nugen, *Lab Chip*, 2015, **15**, 3086–3094.
10 J. H. Chen, Z. W. Jiang, J. D. Ackerman, M. Yazdani, S. Hou, S. R. Nugen and V. M. Rotello, *Analyst*, 2015, **140**, 4991–4996.
11 Y. X. Zhou, B. Yu and K. Levon, *Chem. Mater.*, 2003, **15**, 2774–2779.
12 S. Yaqub, U. Latif and F. L. Dickert, *Sens. Actuators, B*, 2011, **160**, 227–233.
13 P. Lenain, S. De Saeger, B. Mattiasson and M. Hedstrom, *Biosens. Bioelectron.*, 2015, **69**, 34–39.
14 G. Q. Sun, P. P. Wang, S. G. Ge, L. Ge, J. H. Yu and M. Yan, *Biosens. Bioelectron.*, 2014, **56**, 97–103.
15 N. W. Turner, C. W. Jeans, K. R. Brain, C. J. Allender, V. Hlady and D. W. Britt, *Biotechnol. Prog.*, 2006, **22**, 1474–1489.
16 Y. T. Wang, Y. X. Zhou, J. Sokolov, B. Rigas, K. Levon and M. Rafailovich, *Biosens. Bioelectron.*, 2008, **24**, 162–166.
17 Y. T. Wang, Z. Q. Zhang, V. Jain, J. J. Yi, S. Mueller, J. Sokolov, Z. X. Liu, K. Levon, B. Rigas and M. H. Rafailovich, *Sens. Actuators, B*, 2010, **146**, 381–387.
18 M. K. Boehm, M. O. Mayans, J. D. Thornton, R. H. J. Begent, P. A. Keep and S. J. Perkins, *J. Mol. Biol.*, 1996, **259**, 718–736.
19 Y. X. Zhou, B. Yu and K. Levon, *Abstr. Pap. Am. Chem. Soc.*, 2003, **225**, U128–U128.
20 K. Levon, Q. Zhang, Y. Wang, A. Martur and R. Kolli, in *Electrochemical Processes in Biological Systems*, ed. L. Gorton, A. Lewenstam and A. Wieckowski, Wiley, 1st edn, 2015, ch. 9, pp. 213–230.
21 V. Ganesh, S. K. Pal, S. Kumar and V. Lakshminarayanan, *J. Colloid Interface Sci.*, 2006, **296**, 195–203.
22 S. E. Moulton, J. N. Barisci, A. Bath, R. Stella and G. G. Wallace, *J. Colloid Interface Sci.*, 2003, **261**, 312–319.
23 C. Vericat, M. Vela, G. Benitez, P. Carro and R. Salvarezza, *Chem. Soc. Rev.*, 2010, **39**, 1805–1834.
24 M. Cohen-Atiya and D. Mandler, *J. Electroanal. Chem.*, 2003, **550**, 267–276.
25 Q. Zhang, H. S. Majumdar, M. Kaisti, A. Prabhu, R. Österbacka, A. Ivaska, A. Rahman and K. Levon, *IEEE Trans. Electron Devices*, 2015, **62**, 1291–1298.